Geobiology

Geobiology (2009), 7, 373–384 DOI: 10.1111/j.1472-4669.2009.00203.x

Transformation of vivianite by anaerobic nitrate-reducing iron-oxidizing bacteria

J. MIOT,[1] K. BENZERARA,[1] G. MORIN,[1] S. BERNARD,[2] O. BEYSSAC,[2] E. LARQUET,[1] A. KAPPLER[3] AND F. GUYOT[1]

[1]*Institut de Minéralogie et de Physique des Milieux Condensés, Universités Paris 6 et Paris 7, Paris, France*
[2]*Ecole Normale Supérieure, CNRS, Geology Laboratory, Paris, France*
[3]*Geomicrobiology, Center for Applied Geoscience (ZAG), University of Tuebingen, Tuebingen, Germany*

ABSTRACT

In phosphate-rich environments, vivianite ($Fe^{II}_3(PO_4)_2$, $8H_2O$) is an important sink for dissolved Fe(II) and is considered as a very stable mineral due to its low solubility at neutral pH. In the present study, we report the mineralogical transformation of vivianite in cultures of the nitrate-reducing iron-oxidizing bacterial strain BoFeN1 in the presence of dissolved Fe(II). Vivianite was first transformed into a greenish phase consisting mostly of an amorphous mixed valence Fe-phosphate. This precipitate became progressively orange and the final product of iron oxidation consisted of an amorphous Fe(III)-phosphate. The sub-micrometer analysis by scanning transmission X-ray microscopy of the iron redox state in samples collected at different stages of the culture indicated that iron was progressively oxidized at the contact of the bacteria and at a distance from the cells in extracellular minerals. Iron oxidation in the extracellular minerals was delayed by a few days compared with cell-associated Fe-minerals. This led to strong differences of Fe redox in between these two types of minerals and finally to local heterogeneities of redox within the sample. In the absence of dissolved Fe(II), vivianite was not significantly transformed by BoFeN1. Whereas Fe(II) oxidation at the cell contact is most probably directly catalyzed by the bacteria, vivianite transformation at a distance from the cells might result from oxidation by nitrite. In addition, processes leading to the export of Fe(III) from bacterial oxidation sites to extracellular minerals are discussed including some involving colloids observed by cryo-transmission electron microscopy in the culture medium.

Received 14 November 2008; accepted 20 April 2009

Corresponding author: J. Miot. Tel.: (0033)-1 44 27 98 32; fax: (0033)-1 44 27 37 85; e-mail: miot@impmc.jussieu.fr

INTRODUCTION

A huge proportion of ferrous iron found at the Earth surface is immobilized in solid phases. Oceanic crust represents a significant surface reservoir, in which iron is incorporated in diverse minerals, including sulfur minerals such as pyrite (FeS_2) or ferrous sulfide (FeS), titanomagnetite and Fe-silicates (Schippers & Jorgensen, 2002, Edwards *et al.*, 2003). At a distance from the ridge, Fe(II) is progressively oxidized into Fe(III) through abiotic or possibly microbial processes (e.g. Schippers & Jorgensen, 2002). An increasing number of studies have attempted to assess the capabilities of microbes such as iron-oxidizing bacteria to oxidize solid-phase Fe(II) and to use it as a source of energy. However, the mechanisms by which microbes uptake Fe(II) from solid phases are still poorly understood, especially under pH conditions close to neutrality (e.g. Schaedler *et al.*, 2008).

A few phototrophic micro-organisms are known to oxidize soluble Fe(II) at neutral pH under strictly anoxic conditions (e.g. Widdel *et al.*, 1993; Ehrenreich & Widdel, 1994; Heising & Schink, 1998). Additionally, some bacteria use nitrate as an electron acceptor for the oxidation of Fe(II) (Hafenbradl *et al.*, 1996; Straub *et al.*, 1996; Benz *et al.*, 1998; Straub & Buchholz-Cleven, 1998; Kappler *et al.*, 2005), following the reaction (Eqn 1):

$$2Fe^{2+} + 5H_2O + NO_3^- = 2Fe(OH)_3 + 4H^+ + NO_2^- \quad (1)$$

where in the by-product of the soluble Fe(II) oxidation is generically symbolized as Fe(III)-hydroxides $Fe(OH)_3$ for simplicity. While most of the studies on Fe-oxidizing bacteria have used Fe(II) in a soluble form, it has been shown that these bacteria can also enhance the dissolution and oxidation of various solid-phase Fe(II) compounds, such as

siderite ($FeCO_3$), FeS or magnetite (Fe_3O_4) (Weber *et al.*, 2001; Schippers & Jorgensen, 2002; Kappler & Newman, 2004). Such metabolisms might thus play a crucial role in the weathering of Fe(II)-bearing minerals and consequently impact the geochemical cycle of iron and heavy metals in neutral-pH anoxic environments, such as river sediments, lakes or deep-sea environments (e.g. Edwards *et al.*, 2003).

In non-marine environments and at high phosphate concentration, Fe(II) can be in the form of amorphous or crystalline ferrous phosphate. In particular, vivianite ($Fe^{II}_3(PO_4)_2$, $8H_2O$) is considered as one of the most important sinks of P in lakes (Nriagu & Dell, 1974; Buffe *et al.*, 1989; Manning *et al.*, 1991; Fortin *et al.*, 1993; Viollier *et al.*, 1997; Sapota *et al.*, 2006). In some cases, this mineral, which is very stable ($K_S = 10^{-36}$; Nriagu, 1972), can partly control the geochemical cycles of Fe and P and thereby the trophic status of lakes. Illustrating that idea, Fe(II,III) salt additions can be used to efficiently reduce P concentrations in eutrophic environments (see e.g. Frossard *et al.*, 1996). Moreover, phosphate amendments are also commonly used for the remediation of polluted environments: natural phosphate rocks additions in acid mine drainages lead to the immobilization of heavy metals as secondary metal phosphate precipitates within mining wastes (Ueshima *et al.*, 2004). In the same way, vivianite nanoparticles have been shown to be efficient in immobilizing heavy metals in the environment (e.g. Liu & Zhao, 2007). Both treatments influence the precipitation or dissolution of iron-phosphate minerals, which depend on redox conditions, pH, availability of dissolved elements (in particular P and Fe) and organic matter content (Nriagu & Dell, 1974; Manning *et al.*, 1991). All these parameters can be affected by microbial activities, in particular by anaerobic iron bio-oxidation. However, due to its low solubility at neutral pH (Nriagu, 1972), vivianite is supposed to remain very stable under anoxic conditions and it cannot be transformed by anaerobic iron-oxidizing bacteria when this mineral is the only source of Fe(II) (Kappler & Newman, 2004). However, in natural systems, vivianite is usually at equilibrium with a saturated solution.

In the present study, the nitrate-reducing iron-oxidizing bacterial strain BoFeN1 (Kappler *et al.*, 2005) was cultured in the presence of vivianite, initially at equilibrium with a saturated solution and we studied the displacement of this equilibrium driven by iron bio-oxidation. The resulting mineralogical transformations of vivianite and the oxidation of Fe(II)-minerals were followed along the time course of a batch culture down to the nanometer scale, using a combination of transmission electron microscopy (TEM) and synchrotron-based scanning transmission X-ray microscopy (STXM). We evidenced significant mineralogical transformations of vivianite as well as a progressive oxidation of dissolved and solid Fe(II) directly or indirectly driven by bacteria.

MATERIALS AND METHODS

Bacterial strain and growth conditions

The nitrate-reducing Fe(II)-oxidizing strain BoFeN1, isolated from Lake Constance littoral sediments (Kappler *et al.*, 2005), was cultivated in freshwater mineral medium prepared after Ehrenreich & Widdel (1994), containing 4.4 mM phosphate. BoFeN1 was grown in this medium supplemented with 5 mM acetate (provided as sodium acetate) and 10 mM nitrate (provided as sodium nitrate) in the presence or absence of Fe(II) (provided as $FeCl_2$). The addition of Fe(II) at a total concentration of 10 mM led to the precipitation of a white Fe-rich precipitate identified as vivianite by X-ray diffraction (XRD; see Results section) and resulting in a dissolved Fe(II) concentration of ~3 mM. For each culture, 25 mL of medium was transferred into a 58 mL serum bottle that was flushed with N_2/CO_2 (80%/20%), closed with a butyl rubber stopper and crimped. BoFeN1 was inoculated at 10% from an acetate nitrate-grown culture (culture without iron) to prevent the effects of potentially transferred Fe minerals. Cultures were incubated at 30 °C in the dark. For X-ray absorption spectroscopy (XAS), XRD and STXM analyses, samples of the same culture were collected at several time steps in an O_2-free glove-box (pO_2 < 50 p.p.m.).

In a complementary experiment, BoFeN1 was cultured in the presence of vivianite as the sole source of Fe(II) (no dissolved Fe(II)). For this experiment, vivianite was synthesized in the culture medium, sampled, rinsed twice in degassed distilled water, dried under vacuum in an anoxic glove-box and finally added to a fresh culture medium before addition of acetate (5 mM) and nitrate (10 mM) and inoculation of the strain.

Analytical methods

Bacterial growth was followed by measuring the total content of proteins using the Bradford assay (Bradford, 1976). 1 milliliter of culture was mixed with 840 µL of a solution of oxalic acid (pH 3, 0.2 M) in order to dissolve iron-bearing minerals and with 160 µL of 6.1 M trichloroacetic acid to precipitate proteins. After centrifugation (11 000 × *g*, 30 min) and removal of the supernatant, proteins were dissolved in 1 mL of 0.1 M NaOH at 60 °C for 6 min. The absorbance of the samples was measured at 595 nm after reaction with the Bradford reagent (microassay; Bio-Rad, Marnes-la-Coquette, France).

In order to measure the concentration of dissolved iron, 100 µL of a culture suspension or the abiotic control were sampled with a syringe and filtered through 0.22 µm Millipore filter in an anoxic glove-box. The dissolved Fe(II) content of the filtrate was determined by the ferrozine assay (Viollier *et al.*, 2000) after dilution with 900 µL of 1 M HCl. Solid Fe(II) and Fe(III) concentrations could not be

estimated using wet chemical extraction due to incomplete dissolution of vivianite in 6 M HCl, which led to an underestimation of the solid Fe(II) content.

The composition of the culture medium was additionally simulated using the JCHESS software (Van der Lee, 1998) taking into account the complete chemistry of the solution, including pH and gas partial pressures. These simulations provided the theoretical concentrations of the dissolved compounds and the nature of the solid phases precipitating in the medium at the thermodynamic equilibrium and agreed with our measurements.

Synthesis of model compounds

The Fe redox state of the samples was determined at the submicrometer scale by using STXM at the Fe $L_{2,3}$-edges. The Fe(II) and Fe(III) reference end-members used for this study were pure Fe(II)- and Fe(III)-phosphates. Both were synthesized under anoxic conditions. Fe(II)-phosphate was obtained by adding 10 mM Fe(II) (as $FeCl_2$), 5 mM acetate and 10 mM nitrate to the growth medium, which led to the precipitation of a whitish phase identified as pure vivianite by XRD. X-ray amorphous Fe(III)-phosphate was obtained by adding 10 mM Fe(III) (as $FeCl_3$), 5 mM acetate and 10 mM nitrate to the growth medium. Both precipitates were rinsed twice with degassed distilled water and dried under vacuum inside an anoxic glove-box.

Mineral characterization by X-ray diffraction

The mineralogical compositions of the solid phases collected from 4-day and 1-year-old cultures, as well as of the Fe(II)- and Fe(III)-phosphate references were determined by XRD. The whole sample preparation procedure described hereafter was carried out in an anoxic glove-box in order to guarantee strict anoxic conditions for XRD analyses. The cultures were centrifuged ($5000 \times g$, 10 min) and the solid phases were systematically rinsed twice using degassed distilled water and vacuum-dried. The resulting powder was ground in an agate mortar and dispensed in a borosilicate capillary that was sealed with glue before analysis in the diffractometer. XRD measurements were performed with Co*Ka* radiation on a Panalytical® X'Pert Pro MPD diffractometer (PANalytical SAS, Limeil-Brevannes, France) mounted in Debye-Scherrer configuration using an elliptical mirror to obtain a high flux parallel incident beam and an X'Celerator® detector (PANalytical SAS) to collect the diffracted beam. Data were recorded in the continuous-scan mode within the 5–90° 2θ range with a step of 0.03°, and a counting time of 12–24 h per sample.

Bulk XAS analyses

The XAS data were acquired on the products of Fe(II) bio-oxidation by BoFeN1 at the Fe K-edge. Samples were transferred from the glove-box into a liquid nitrogen bath and then into the cryostat, where they were placed under He atmosphere. This procedure preserved anoxic conditions during sample transfer and analysis. The data were recorded on beamline 10-2 at the Stanford Synchrotron Radiation Laboratory (SSRL) using a Si(220) double-crystal monochromator. Due to the low amount of sample available, data were collected on samples mixed with cellulose, in fluorescence detection mode using a 13-element Ge-array detector and a 3 $\Delta\mu$ Mn filter to attenuate elastic scattering. Energy was calibrated by using a double-transmission setup; the first inflection point of the Fe metal foil K-edge was set at 7111.1 eV (Wilke *et al.*, 2001). In order to limit Fe(III) reduction under the X-ray beam and to enhance EXAFS signal on our nano-sized and poorly-ordered mineral phases, all data were recorded at 10–15 K using a modified Oxford® liquid He cryostat (Oxford Instruments, Saclay, France). Details on the experimental setup and on data acquisition for the reference samples are given in the Supporting Information.

X-ray absorption spectra were averaged using the SIXPACK software (Webb, 2004). EXAFS data were extracted using the XAFS program (Winterer, 1997) and were fit following classical procedures, as detailed previously in Miot *et al.*, 2008 (see Supporting Information).

Analytical transmission electron microscopy

For conventional TEM and energy dispersive X-ray spectrometry (EDXS) measurements, a drop of the culture medium was deposited and dried on a carbon-coated 200-mesh copper grid after two rinses in degassed distilled water within an anoxic glove-box.

For cryo-electron microscopy observations, the sample was transferred onto grids covered with holey carbon films and then vitrified by flash freezing in liquid ethane (Adrian *et al.*, 1984). Images were recorded under low-dose conditions (10 electrons per $Å^2$) on a GATAN Ultrascan 1000 CCD Camera (Grandchamp, France).

Observations and EDXS analyses were performed with a JEOL2100F microscope (JEOL Europe SAS, Croissy sur Seine, France) operating at 200 kV equipped with an Si(Li) diode. P/Fe atomic ratios were estimated from the EDXS spectra using the IDFIX software.

TEM was thus used for imagery and elemental analysis but not for the determination of Fe redox state that could not be preserved under these experimental conditions. Redox state of iron was determined using STXM (see below).

Scanning transmission X-ray microscopy

Sample preparation

We kept the samples under an anoxic atmosphere from preparation to transfer into the microscope, following the method detailed in Miot *et al.* (2008). The entire preparation was

performed in an anoxic glove-box. One milliliter of a suspension of BoFeN1 culture (or of reference compounds) was sampled at different stages of each culture (30 min to 6 days, and 1 year). Each sample was rinsed twice in degassed distilled water. 0.3 μL of each sample was sandwiched in between two silicon nitride membranes (Norcada Inc., Edmonton, Canada) that were sealed under the anoxic atmosphere using epoxy. Using this protocol, we verified that we could preserve the original redox state of iron of vivianite.

STXM experiments

The STXM observations at the Fe $L_{2,3}$-edges were performed on the PolluX beamline at the Swiss Light Source (SLS; Villigen). Additional information on the PolluX beamline can be found in Bernard *et al.* (2007). This beamline has an energy resolving power ($E/\Delta E$) superior to 3000. Energy calibration was achieved using the major absorption peak of hematite at 708.7 eV for the Fe L_3-edge.

Data processing

Image stacks were acquired at the Fe $L_{2,3}$-edges. They were performed by scanning the sample in the x–y direction at each energy increment over the energy range of interest. Potential sample damages caused by the incident photon beam (i.e. changes in the Fe redox state) were quantified by monitoring spectral changes at the Fe $L_{2,3}$-edge with increasing dwell times up to several tens of milliseconds (Fig. S1). However, no significant change was observed for typical dwell times used during analyses of the samples (i.e. around 0.8 ms per energy- and image-point). The aXis2000 software-package (Hitchcock, 2001) was used for processing image stacks and XANES spectra. Images were recorded on transmission scale and converted into optical density (OD) according to Eqn (2).

$$\mathrm{OD} = -\ln(I/I_0) \quad (2)$$

where I represents the measured photon intensity at the point of interest and I_0 represents the intensity outside the sample that includes the absorption by silicon nitride windows.

Quantitative Fe-speciation maps were calculated from the image stacks by singular value decomposition using the stack-fit routine in aXis2000. The algorithm fits the spectra of each individual pixel with a linear combination of the two normalized reference spectra (Fe(II)- and Fe(III)-phosphate model compounds) plus a constant, accounting for the absorption background. Composite maps were obtained by overlaying on the same image the Fe(II) (blue) and the Fe(III) (red) maps using a common intensity scale for both color channels.

XANES spectra were extracted from the stacks on regions of interest. We normalized the area below the L_2 and L_3 edges to 1 and multiplied the absorbance of the compounds containing mainly Fe(II) (major peak at 707 eV) by a 4/5 correction factor to take into account the difference in the occupancy of the 3d orbitals in Fe^{2+} and Fe^{3+} ions, neglecting the variation of radial integrals (Thole *et al.*, 1994). We fitted the normalized spectra with linear combinations of the normalized reference spectra of the Fe(II)-phosphate model compound (vivianite) and of the 1-year-old BoFeN1 sample standing for a Fe(III)-reference, applying the conjugate gradient optimization method curve fit routine in Axis2000. Fit results allowed estimating the Fe(III)/Fe(total) content of regions of interest. Standard deviations calculated from the deviation between the fit and the data were systematically less than 1%. Moreover, Fe(II) and Fe(III) maps were used to evaluate the variability of the Fe(III)/Fe(total) ratio within each sample (i.e. at each stage of the culture): the Fe(II)-map was multiplied by the 4/5 correction factor (see above) and added to the Fe(III)-map to obtain a Fe(total) map. The Fe(III)-map was subsequently divided by the Fe(total) map. An histogram of the resulting map was plotted, giving the number of pixels as a function of Fe(III)/Fe(total) ratio. These histograms allowed discriminating the different populations of Fe according to their redox state within the image. The mean Fe(III)/Fe(total) ratios were calculated as the maxima of each peak in the histogram and the variability as the width at mid height of the peak.

RESULTS

XRD and XAS study of mineralogical transformations of vivianite in BoFeN1 cultures

Addition of 10 mM Fe(II) to the culture medium before inoculation of BoFeN1 led to the instant precipitation of a white mineral phase (Fig. 1A) characterized by XRD as vivianite (Fig. 2). This phase was at the equilibrium with the solution that contained around 2.5 mM dissolved Fe(II), consistently with thermodynamic calculations taking into account the medium culture composition and the solubility of vivianite ($[Fe^{2+}]_{eq}$ = 3.4 mM as indicated by JChess (Van der Lee, 1998) simulations, using the EQ3.6 database). The concentration of dissolved Fe(II) remained constant over the period of the experiment in the abiotic control, whereas it dropped to undetectable levels within 6 days in BoFeN1 cultures (Fig. 1B). Dissolved Fe(II) consumption (oxidation) was related to bacterial growth, with the stationary phase starting after 3 days of culture. Moreover, the progressive oxidation of dissolved Fe(II) was associated with a macroscopic change in the color of the precipitate from white initially (vivianite) to green after 4 days of culture and finally orange after 16 days (Fig. 1A), whereas no change in color was observed in abiotic controls, in which the precipitate remained white.

XRD analyses were performed on the successive phases formed in these cultures in order to better understand this change in color of the precipitates. These analyses revealed the progressive transformation of crystalline vivianite into an amorphous compound (as shown by the disappearance of the peaks characteristic of vivianite in the XRD pattern of the

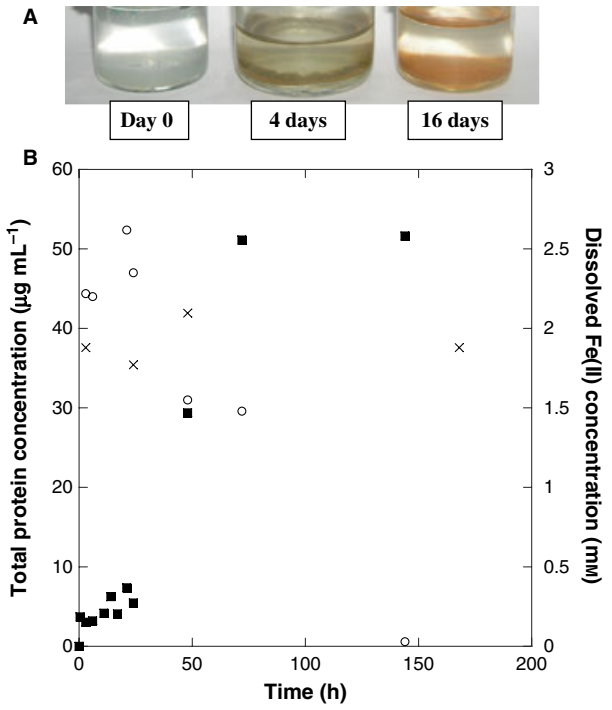

Fig. 1 Growth of BoFeN1 in the presence of vivianite. (A) Evolution of the color of the precipitates forming in the culture medium, before inoculation (Day 0, white vivianite precipitate) and after 4 and 16 days of incubation. (B) Growth curve of BoFeN1 and dissolved Fe(II) concentration in the presence of acetate (5 mM), nitrate (10 mM), dissolved ferrous iron and vivianite over a period of 7 days. (■): Total protein concentration, (○): Dissolved Fe(II) concentration in the BoFeN1 culture, (X): Dissolved Fe(II) concentration in the abiotic control.

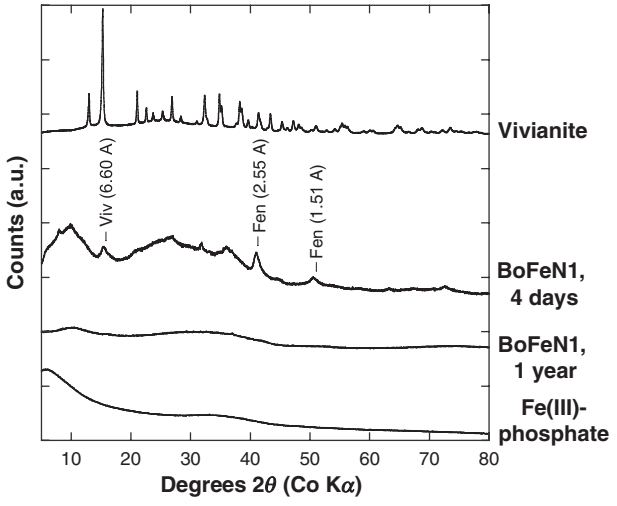

Fig. 2 X-ray diffractograms of precipitates collected from BoFeN1 cultures before inoculation (Day 0, reference Fe(II)-phosphate mineral), after 4 days and 1 year of incubation and of reference Fe(III)-phosphate. All peaks of the reference Fe(II)-phosphate (Day 0) are explained by vivianite. Viv, vivianite; Fen, Fe(III)-oxyhydroxynitrate ($FeO(NO_3)_x(OH)_{1-x}$).

1-year-old sample, Fig. 2). The intermediate greenish phase (4-day-old precipitate) was mostly amorphous. Although some Bragg peaks were present, they could not be attributed unequivocally to any known mineral phase, except for a broad peak consistent with poorly ordered vivianite at 6.6 Å and two peaks at 2.25and 1.51 Å that could be consistent with the XRD pattern of $FeO(NO_3)_x(OH)_{1-x}$, which is a poorly ordered compound with an akaganeite-like structure (Schwertmann *et al.*, 1996). All these different amorphous phases were further characterized by XAS at the Fe K-edge (Fig. 3 and Table 1). Absorption maxima in the pre-edges of the 4-day-old BoFeN1 sample were observed at 7111.8 and 7113.7 eV, suggesting the coexistence of Fe(II) and Fe(III) oxidation states after 4 days of culture (Fig. 3; Wilke *et al.*, 2001). In the 16-day-old and the 1-year-old samples, the position of the pre-edge at 7113.7 eV indicated the transformation into a mostly Fe(III) mineral, consistently with the shift of 2 eV in the absorption maximum of the XANES spectrum compared to the vivianite model compound. Best fits of the EXAFS data of the BoFeN1 samples are compared to those of the end-members amorphous Fe(III)-phosphate and vivianite in Fig. 3C,D. Corresponding parameters are listed in Table 1. The first-neighbor shell in EXAFS data of the 4-day and the 1-year-old BoFeN1 cultures was fitted with oxygen ligands at 2.08 ± 0.05 and 1.98 ± 0.05 Å, respectively. The second-neighbor shell of these two samples was fitted with phosphorus ligands at 3.32 ± 0.05 and 3.23 ± 0.05 Å, respectively. These distances are consistent with those measured in vivianite and in the amorphous Fe(III)-phosphate, respectively (Table 1). The 16-day-old sample was fitted with intermediate distances. The absence of Fe-Fe pairs at a distance of 3.0–3.2 Å, corresponding to edge-sharing FeO_6 octahedra that are the structural basis of all iron oxyhydroxides, rules out the possibility that the Fe(III) end-product would be an iron oxyhydroxide with adsorbed phosphate. If present, such phases, as well as the hypothetical Fe(III) oxyhydroxynitrate, would necessarily be present in minor proportion (<30% given the detection limit of XAS methods). All these results suggest the progressive transformation of vivianite into an amorphous Fe(III)-phosphate.

TEM study of mineralogical transformations of vivianite in BoFeN1 cultures

TEM observations were performed at the same successive stages of the culture to determine the spatial relationships existing between the bacterial cells and extracellular vivianite. In BoFeN1 cultures, we observed the coexistence of extracellular and cell-associated iron-rich precipitates. Both had a composition of Fe-phosphates. Precipitates associated with the bacteria were similar to those previously described in BoFeN1 cultures grown in the presence of dissolved Fe(II) only (Fig. S2; Miot *et al.*, 2008) and consisted of periplasmic precipitates and surface-bound globules. The morphology and chemical composition of the extracellular minerals were investigated by TEM, Cryo-TEM and EDXS (Fig. 4). In

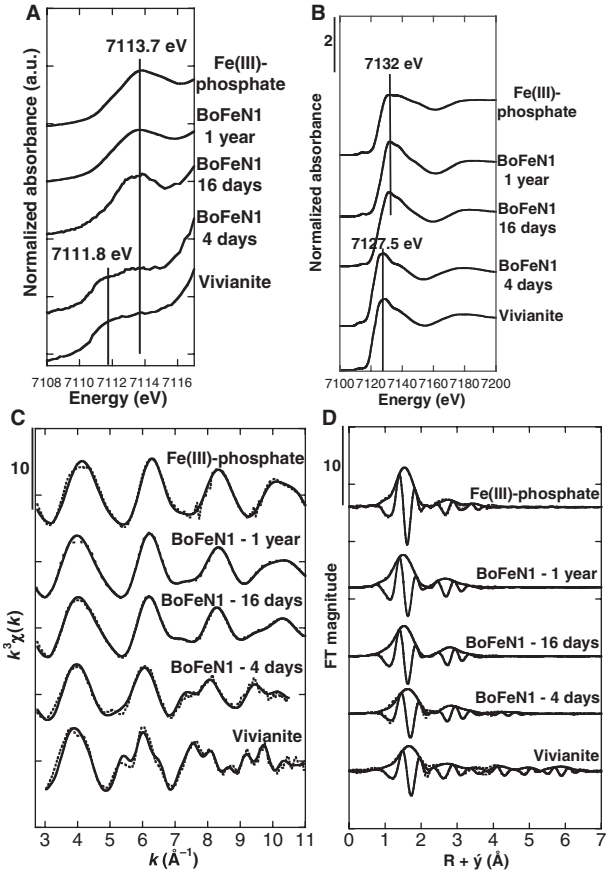

Fig. 3 X-ray absorption spectroscopy measurements on the bulk cultures of BoFeN1 after 4 days, 16 days and 1 year. (A, B) Pre-edges and whole XANES spectra at the Fe K-edge of 4-day, 16-day and 1-year-old BoFeN1 cultures and of Fe(III)-phosphate and vivianite model compounds. (C) unfiltered $k^3\chi(k)$ data compared with the spectra of the model compounds Fe(III)-phosphate and vivianite. (D) Corresponding Fourier Transforms. Dashed lines show the data and solid lines the best fits of the $k^3\chi(k)$ data (see Table 1).

Table 1 Fitting results for Fe K-edge EXAFS data of 4-day-old, 16-day-old and 1-year-old BoFeN1 cultures and of the two-line ferrihydrite, Fe(II)- and Fe(III)-phosphate model compounds. Coordination number (N), interatomic distance (R), Debye-Waller parameter (σ) and energy offset (E_0). Fit quality was estimated by a reduced χ^2 parameter (see text)

Sample	N (±0.3)	Bond	R (Å) (±0.05)	σ (Å) (±0.02)	E_0 (eV) (±3)	χ^2
Fe(III)-phosphate	3.3	Fe-O	1.98	0.06	8	15
	1.0	Fe-P	3.24	0.06	–†	
	0.5	Fe-Fe	3.62	–	–	
BoFeN1, 1 year	4.0	Fe-O	1.98	0.09	2	5
	1.7	Fe-P	3.23	0.08	–	
	0.2	Fe-Fe	3.57	–	–	
BoFeN1, 16 days	3.6	Fe-O	1.98	0.09	6	3
	1.6	Fe-P	3.29	0.08	–	
	0.2	Fe-Fe	3.60	–	–	
BoFeN1, 4 days	3.5	Fe-O	2.08	0.09	10	52
	1.0	Fe-P	3.32	0.05	–	
	0.2	Fe-Fe	3.66	–	–	
	0.5	Fe-Fe	4.81	–	–	
Vivianite	3.8	Fe-O	2.10	0.10	10	7
	1.5	Fe-P	3.30	0.08	–	
	0.4	Fe-Fe	2.96*	–	–	
	1.9	Fe-O	3.97*	–	–	
	1.7	Fe-Fe	4.70*	–	–	
	2.0	Fe-Fe	5.25*	–	–	
	4.3	Fe-Fe	6.29	–	–	

*Fixed at values expected from the structure of vivianite (Fejdi *et al.*, 1980).
†Kept equal to the free parameter placed above in the table.

abiotic controls, we observed vivianite platelets exhibiting a P/Fe atomic ratio estimated to 0.75 ± 0.08 by EDXS, which is consistent with the stoichiometry of vivianite ($Fe_3(PO_4)_2$, $8H_2O$, theoretical P/Fe = 0.67). In the presence of bacteria, the P/Fe ratio of the extracellular minerals dropped to 0.55 ± 0.12 after 2 days and to 0.36 ± 0.15 after 2 months. In addition, we observed that these extracellular minerals kept a platelet morphology. These TEM observations are thus consistent with XRD and XAS analyses, suggesting the progressive transformation of vivianite platelets into an amorphous Fe(III)-phosphate phase exhibiting a P/Fe ratio of 0.36 ± 0.15.

Moreover, after 2 days of incubation, colloidal particles (diameter <10 nm) were observed at the surface of the platelets (Fig. 4B). Moreover, the <100 nm mineral fraction was imaged by cryo-TEM on a BoFeN1 culture frozen in a 100-nm thick film of amorphous ice (Fig. 4C). This preparation retained only the <100 nm fraction of the culture. After exposure to the electron beam and subsequent sublimation of the vitreous ice, we were able to detect numerous colloids in the culture medium, with a diameter of 5.9 ± 1.7 nm. These colloids were present at the surface of the vivianite platelets or unattached in the culture medium. Direct EDXS analyses of these colloids under cryo-conditions revealed that they also had a composition of iron phosphates (Fig. 4D). All these results indicate that in parallel to the transformation of the vivianite platelets, iron-phosphate colloids are present in BoFeN1 cultures.

Fe oxidation at the nanometer scale in BoFeN1 cultures

The temporal evolution of iron redox state in extracellular as well as in cell-associated precipitates was analyzed in BoFeN1 cultures at the sub-micrometer scale by STXM analyses at the Fe $L_{2,3}$-edges (Fig. 5). The redox state of iron measured on bacteria represents a mean of the redox states of iron in the periplasmic and the surface-bound precipitates as these two mineral phases cannot be distinguished with the spatial resolution of STXM (~25 nm). As shown on Fe(II)-Fe(III) maps, bacteria and extracellular precipitates both contained mainly Fe(II) at the beginning of the culture (30 min) and both became progressively oxidized over the course of the culture (Fig. 5). However, as shown on histograms (Fig. 6), the extracellular precipitates and the bacterial cells could be

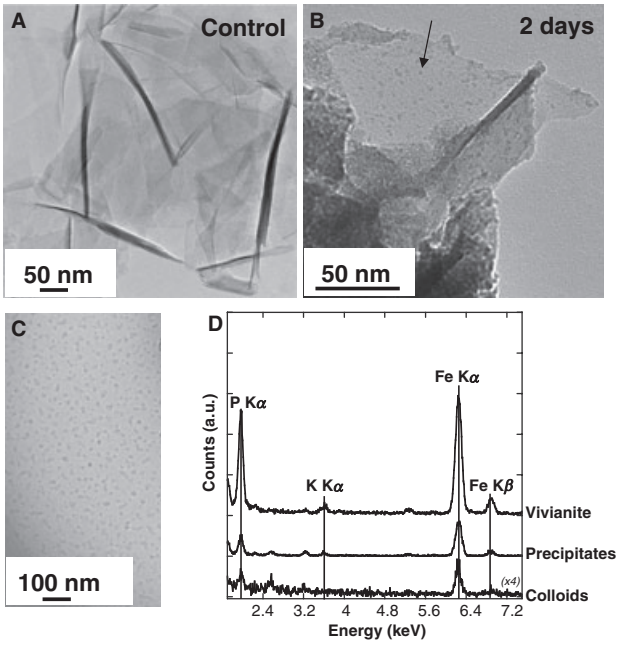

Fig. 4 Electron microscopic study of Fe-rich minerals forming in BoFeN1 cultures. (A) TEM image of vivianite precipitates forming in the non-inoculated culture medium. (B) TEM image of iron-phosphate minerals in a 2-day-old culture of BoFeN1. The arrow points to colloids at the surface of the platelets. (C) Cryo-TEM image of colloids in a 15-day old BoFeN1 culture. (D) XEDS spectra measured on vivianite (abiotic control) and on extracellular precipitates and colloids (spectrum multiplied by a factor 4) from a BoFeN1 culture.

discriminated at each time point according to their redox state: the extracellular precipitates exhibited a lower Fe(III)/Fe(total) ratio than the Fe-precipitates associated with bacteria. Moreover, the Fe(III)/Fe(total) ratio measured on bacteria evolved from 0.28 ± 0.19 (here deviation represents the intrinsic variability within the sample) after 3 h to 0.94 ± 0.22 after 6 days of culture, indicating that iron associated with bacteria was completely oxidized after 6 days of culture. In contrast, the Fe(III)/Fe(total) ratio measured on extracellular precipitates evolved from 0.18 ± 0.13 after 3 h towards 0.50 ± 0.2 after 6 days of culture, i.e. a fairly homogenous mixed-valence iron phase. Similar estimations could be drawn by direct fitting of the XANES spectra extracted from bacteria and extracellular precipitates, respectively (Fig. 6A,B and Table 2). All these results indicate that iron oxidation rate is slower in the extracellular precipitates than at the cell contact.

In summary, our results indicate the progressive transformation of vivianite $Fe^{II}_3(PO_4)_2$, 8 H_2O into (1) a green phase consisting of amorphous platelets composed of mixed valence Fe-phosphate, with a P/Fe atomic ratio of 0.55 and eventually into (2) an orange phase consisting of an amorphous Fe(III)-phosphate mineral in the form of platelets, with a P/Fe atomic ratio of 0.36. Additionally, iron phosphate colloids were observed all along the culture. Finally, the oxidation rate of iron was higher at the point of cell contact than on the extracellular precipitates.

DISCUSSION

Mineralogy of the oxidation products of vivianite in BoFeN1 cultures

Vivianite was progressively transformed into an amorphous Fe(III)-phosphate in BoFeN1 cultures (Figs 2 and 3). This was documented by a progressive decrease in the vivianite diffraction peaks in XRD (Fig. 2), by a change in the P/Fe ratio measured by EDXS on the precipitates formed in the cultures (Fig. 4) and finally by the progressive change in the Fe-redox state documented by XAS both at the bulk (Fig. 3)

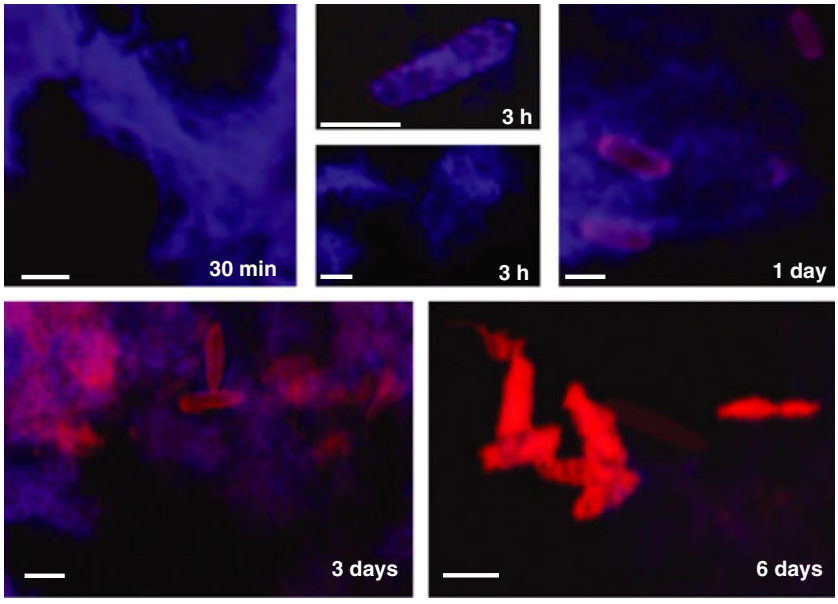

Fig. 5 Evolution of iron redox state 30 min to 6 days after inoculation. Fe redox mapping after 30 min (extracellular precipitates mostly composed of Fe(II)), 3 h (bottom: extracellular precipitates mostly composed of Fe(II), top: Fe-encrusted cell containing mainly Fe(II)), 1 day [Fe(II)-rich extracellular precipitates (blue) and bacteria encrusted by mixed-valence Fe minerals (pink)], 3 days [extracellular minerals composed of mixed-valence iron and bacteria encrusted by minerals enriched in Fe(III) (red)] and 6 days of incubation (extracellular precipitates containing mixed-valence iron and Fe(III) encrusted bacteria). Scale bars: 1 μm.

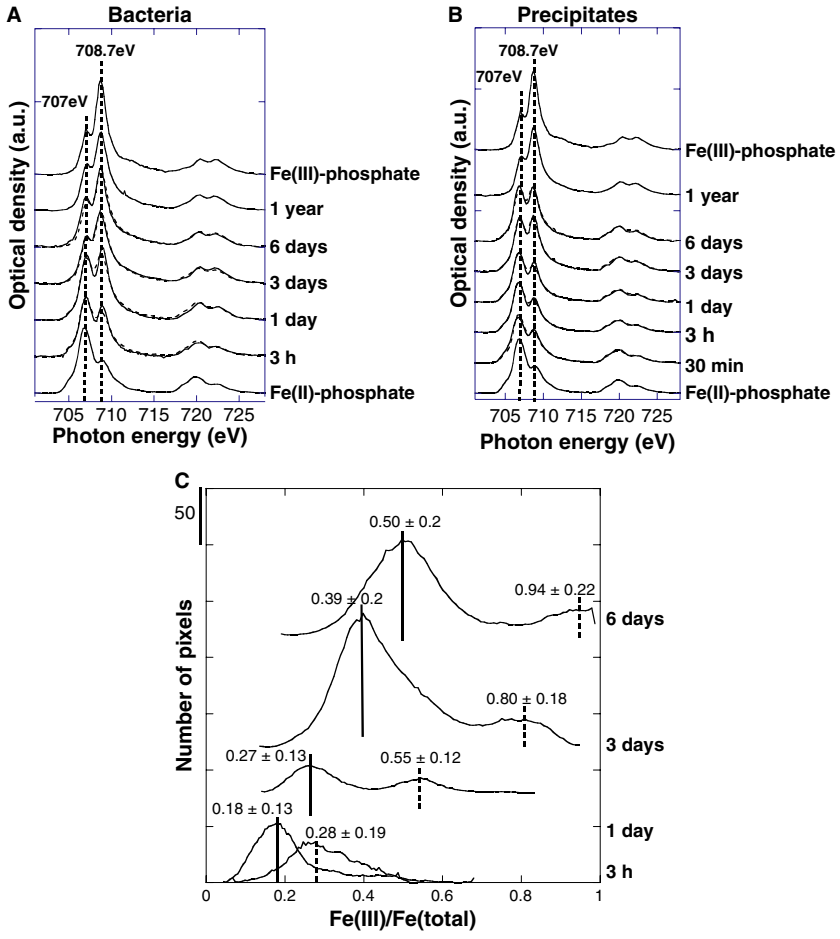

Fig. 6 (A, B) XANES spectra at the Fe $L_{2,3}$-edge obtained on bacteria and extracellular precipitates, respectively, collected on 30 min-old to 6-day-old and 1 year-old cultures. Solid lines show the data and dashed lines the best fits. The numerical results of the fits are displayed in Table 2. (C) Histograms obtained from the Fe(II) and Fe(III) stack maps, giving the Fe(III)/Fe(total) ratio on precipitates (solid lines) and bacteria (dashed lines), respectively. Numbers indicated on the plot are the means ± the width at mid-height of the peaks.

Table 2 Fe(III)/Fe(total) quantification obtained from the fit of Fe $L_{2,3}$-edge XANES spectra extracted from stacks on bacteria and precipitates at different stages of the culture. Fe(III)/Fe(total) values result from at least two spectra fits

Area	Time	Mean Fe(III)/Fe(total)
Bacteria	3 h	0.27
	1 day	0.65
	3 days	0.91
	6 days	0.99
Precipitates	0.5 h	0.17
	3 h	0.17
	1 day	0.26
	3 days	0.59
	6 days	0.62

and at the submicrometer scale (Figs 5 and 6). An intermediate greenish iron-phosphate solid, identified after 4 days of culture, exhibited a mixed Fe oxidation state, as assessed by XAS (Figs 2 and 5; Tables 1 and 2). The homogeneity of the Fe redox state and of the P/Fe ratio at the few-nanometer scale suggests that this solid consists of a single phase or of a mixture of multiple phases that appears homogeneous at the few-nanometer scale. In contrast, no greenish phase was identified when BoFeN1 was cultured in the presence of dissolved Fe(II) only (Miot *et al.*, 2008), suggesting that this green precipitate is a specific (intermediate) product of vivianite transformation. XRD pattern of the 4-day-old sample was dominated by very broad diffusion bands corresponding to nanocrystalline or amorphous material and exhibited two broad peaks that could be consistent with the XRD pattern of $FeO(NO_3)_x(OH)_{1-x}$, which is a poorly ordered compound with an akaganeite-like structure (Schwertmann *et al.*, 1996). If present, such a phase would modify the availability of nitrate in the medium. Unfortunately, due to its ill-defined XRD pattern, this phase could not be identified unambiguously in our samples and more investigations will be needed in the future to assess its presence.

Interestingly, a gray-greenish phase has been previously identified by XRD as a carbonate-bearing green rust in cultures of the nitrate-reducing iron-oxidizing bacteria *Dechlorosoma suillum* in the presence of soluble Fe(II) (Chaudhuri *et al.*, 2001). In contrast, the end-product of iron-bio-oxidation by BoFeN1 did not exhibit the characteristic XRD pattern of green rust (Fig. 2). The broad peak at

d = 10.5 Å (2θ = 9.8°) could correspond to the (003) peak of a phosphate-exchanged carbonate green rust, wherein phosphate partially replaces carbonate groups in the interlayer, leading to a wider layer spacing (Hansen & Poulsen, 1999). However, the resonance (006) peak was not observed in our diffraction patterns. Thus, it is more likely that the broad band at d = 10.5 Å is due to an amorphous Fe-phosphate compound. It is likely that under our culture conditions, the high P/Fe ratio in the system inhibited the precipitation of green rust and favored the precipitation of an amorphous Fe-phosphate as end-product of vivianite transformation.

The green mixed-valence phase eventually turned progressively orange as Fe became completely oxidized. This final product of iron bio-oxidation consisted of an amorphous Fe(III)-phosphate as indicated by XRD and EXAFS results (Figs 2 and 3; Table 1) similar to the one formed in BoFeN1 cultures in the presence of dissolved Fe(II) only (Miot *et al.*, 2008). The artifactual transformation of vivianite into an amorphous phase by exposure to air can be ruled out, given the precautions taken during all the experiments to preserve the Fe redox state from the culture to the analyses. Moreover, this final product is structurally close to our reference Fe(III)-phosphate (Fig. 3 and Table 1) and exhibits structural similarities with the natural oxidation product of vivianite, namely santabarbaraite (Pratesi *et al.*, 2003). According to the Fe-P and Fe-Fe distances at 3.25 and 3.6 Å identified in the present study, the structure of this amorphous Fe(III)-phosphate phase is similar to that of amorphous Fe(III)-arsenate recently reported by Paktunc *et al.* (2008), where arsenate tetrahedra share corners with chains of corner-sharing FeO_6 octahedra. The absence of Fe-Fe bonds by edges (at 3.0–3.2 Å) that are the basis of all iron oxyhydroxides rules out the possibility that this phase be an iron oxyhydroxide with adsorbed phosphate. In contrast, our EXAFS results clearly indicate that the final Fe-oxidation product in BoFeN1 cultures consists of a mixed Fe-PO_4 hydroxide consistent with microscopy observations.

Mechanisms of bacteria-mediated oxidation of vivianite

Previous works have investigated the oxidation of dissolved Fe(II) by anaerobic Fe(II)-oxidizing bacteria (Miot *et al.*, 2008; Schaedler *et al.*, 2008). Additionally, several previous studies have shown that the capability of a bacterial strain to oxidize Fe(II) present in a solid phase depends on different parameters related to the solution chemistry and to the mineralogy of the solid phase, and primarily to the solubility. For instance, nitrate-reducing iron-oxidizing bacteria were shown to catalyze the oxidation of FeS_2 at slightly acidic pH values, based on NO_3^- and SO_4^{2-} profiles (Postma *et al.*, 1991; Engesgaard & Kipp, 1992), whereas no bio-oxidation of FeS_2 was observed at pH 8 in a saline medium (Schippers & Jorgensen, 2002). In contrast, FeS oxidation has been reported under the latter conditions in the presence of nitrate-reducing iron-oxidizing bacteria (Schippers & Jorgensen, 2002), as well as in cultures of photoautotrophic iron-oxidizing bacteria at neutral pH (Kappler & Newman, 2004). However, the same phototrophic strains were not able to oxidize magnetite, pyrite or vivianite, which was suggested to result from the high insolubility of these minerals (Kappler & Newman, 2004). In the present study, when BoFeN1 was cultured in the presence of vivianite as the sole source of Fe(II) (no dissolved Fe(II)), no significant dissolution nor transformation of vivianite could be observed (data not shown), which is consistent with its very low solubility product (Nriagu, 1972). In contrast, in the presence of both vivianite and dissolved Fe(II) (~2.5 mM), vivianite was transformed within 16 days into an amorphous Fe(III)-phosphate, which kept the platelet morphology of vivianite (Fig. 3 and Table 1). No transformation of vivianite was observed in non-inoculated sterile media over the duration of the experiment and hence bacterial activity is directly or indirectly responsible for vivianite transformation and oxidation.

In addition, composite Fe(II)-Fe(III) maps indicate that iron oxidation started on the bacteria, very early after inoculation (a few hours). After 3 days of incubation, iron associated with bacteria was almost completely oxidized, whereas the oxidation of extracellular minerals (i.e. initially vivianite) was delayed with respect to cell-associated iron, with only 50 ± 20% of iron oxidized in the extracellular minerals after 6 days against 94 ± 22% on the bacteria (Table 2). However, the progressive increase in the Fe(III)/Fe(total) ratio that is observed in the extracellular mineral phases questions the mechanisms that could transport Fe(III) to the extracellular minerals or oxidize Fe(II) *in situ* in these minerals.

The persistence of the platelet morphology of the initial vivianite over the time course of the culture suggests a replacement of vivianite by amorphous Fe(III)-phosphate. This preservation of morphology during the transformation of one solid phase into another can be interpreted either as a mechanism of solid-state transformation or as a transformation of a solid in the presence of a fluid phase by interface-coupled dissolution-reprecipitation (Putnis & Putnis, 2007). As BoFeN1 cells were not able to transform vivianite in the absence of dissolved Fe(II), the transformation of vivianite cannot be attributed to a dissolution-precipitation process driven by an undersaturation of the culture medium with respect to vivianite. Thus, the following scenario can be proposed.

Extracellular vivianite is oxidized by an oxidant produced by BoFeN1 cells. As no oxidation is observed in abiotic nitrate-rich controls over several days, oxidation by nitrate can be discarded. Nitrite, which has been shown to form as a product of nitrate reduction in BoFeN1 cultures (Kappler *et al.*, 2005), can be considered. Kappler *et al.* (2005) performed bulk measurements of nitrogen species in cultures of BoFeN1 in the presence of dissolved Fe(II) only (no vivianite) and demonstrated that BoFeN1 cells mediate Fe(II) oxidation around seven times faster than nitrite. In the present study, we observe that Fe(II) oxidation on the cells is around three to

five times faster than in extracellular precipitates. All these results can be reconciled in the following scenario: dissolved Fe(II) is directly oxidized by the cells, while Fe(II) in vivianite is oxidized by nitrite produced by BoFeN1. This is supported by two additional observations: (1) vivianite transforms into a greenish phase in purely abiotic experiments where nitrite has been added at a concentration (3 mM) close to the concentration resulting from nitrate reduction in BoFeN1 cultures (data not shown). (2) When BoFeN1 is cultured in the presence of vivianite as the sole source of Fe(II) and acetate as a source of carbon, vivianite is not transformed. This could be explained by the fact that nitrite is formed only when Fe(II) oxidation occurs and not as long as only acetate is oxidized (Kappler *et al.*, 2005). Hence, while oxidation of dissolved Fe(II) on the cells results from a direct cellular catalysis, solid-phase Fe(II) oxidation outside the cells might result from oxidation by nitrite.

In addition, some Fe(III) may be exported from the cells. In that case, two scenarios have been proposed in the literature to explain how Fe(III), which is very insoluble at neutral pH, can be transported to the extracellular medium (Schaedler *et al.*, 2008): (1) a previous study on the phototrophic iron-oxidizing bacteria *Rhodobacter ferrooxidans* sp. strain SW2 (Kappler & Newman, 2004) suggested that a local drop in pH around the cells may favor Fe(III) export. In the present case, this local drop in pH would also enhance vivianite dissolution. (2) Kappler & Newman (2004) suggested a release of Fe(III) from the cells as an inorganic aqueous complex and/or as a colloidal aggregate. In the present work, we show the presence of 5.9 ± 1.7 nm-sized iron-phosphate colloids in BoFeN1 cultures. Although it was not possible to determine the iron redox state of these colloids (due to their small size), we suggest that they could play a role in Fe(III) export from the bacteria to the extracellular minerals. They may form at the surface of the cells, then diffuse in the solution, aggregate and serve as mineral nucleation sites once a critical size has been reached (Von Guten & Schneider, 1991). Sorption and aggregation of these colloids at the surface of vivianite accompanied by a progressive dissolution of vivianite could lead to the replacement of this Fe(II) mineral by an amorphous Fe(III)-phosphate preserving the platelet morphology.

In any case, our results suggest that vivianite transformation is mostly driven by bacteria indirectly (i.e. involvement of nitrite). Whether those micro-organisms can retrieve some energy from the oxidation of Fe(II) in vivianite remains an open question. We observed that the total protein concentration reached in stationary phase (Fig. 1) was not very different from the concentration obtained in cultures performed in the presence of dissolved Fe(II) only and in the absence of solid-phase Fe(II) (Miot *et al.*, 2008). This could support the fact that vivianite is not directly used by the cells as an energy source. Further investigations, including a complete mass balance of the chemical species involved in the bacterial metabolism, are needed to verify this hypothesis.

CONCLUSIONS

In the presence of vivianite and dissolved Fe(II), BoFeN1 cells used rapidly dissolved Fe(II) but also had the capability to drive the complete transformation of vivianite into an amorphous Fe(III)-phosphate. Nitrite resulting from metabolic reduction of nitrate (using the electron stemming from the organic co-substrate acetate) might be responsible for the oxidation of this Fe(II)-bearing solid-phase. In addition, colloidal iron-phosphate observed in this system might play a role in the extracellular transfer of Fe(III) to the solid phases. Similar Fe-phosphate colloids have been rarely reported in natural environments (e.g. Buffe *et al.*, 1989). This colloidal fraction could have been overlooked so far and has to be studied in more detail given its potentially important role in controlling the mobility of Fe(III) at neutral pH and therefore the Fe cycling (Sobolev & Roden, 2002). In addition, the delay of Fe oxidation in extracellular minerals compared to Fe associated with bacteria leads to redox heterogeneities at the sub-micrometer scale. Such redox heterogeneities corresponding to biological micro-environments have been previously described in natural systems (e.g. Benzerara *et al.*, 2005, 2007) and could be tested as signatures of such metabolisms in present environments or in the geological record.

ACKNOWLEDGEMENTS

The authors are indebted to the SSRL staff, especially Serena DeBeer George, and Mike Toney for their technical assistance during the XAS experiments. We thank Joerg Raabe and George Tzvetkov for their help with STXM experiments on the Pollux beamline at SLS. The authors also thank the SSRL, LURE, SOLEIL and ESRF synchrotron facilities for having provided beamtime for this study. This work was supported by the ECCO/ECODYN CNRS/INSU Program, by ACI/FNS grant #3033, by SESAME IdF grant #1775 and by NSF-EMSI Grant CHE-0431425 (Stanford Environmental Molecular Science Institute). This work was also supported by an Emmy-Noether fellowship from the German Research Foundation (DFG) to Andreas Kappler. We are also grateful to Region Ile-de-France for convention SESAME 2000 E1435 for the support to cryo-electron microscope JEOL 2100F installed at IMPMC UMR 7590. This is IPGP contribution 2520.

REFERENCES

Adrian M, Dubochet J, Lepault J, MacDowall AW (1984) Cryo-electron microscopy of viruses. *Nature* **308**, 32–36.

Benz M, Brune A, Schink B (1998) Anaerobic and aerobic oxidation of ferrous iron at neutral pH by chemohetereotrophic nitrate-reducing bacteria. *Archives of Microbiology* **169**, 159–165.

Benzerara K, Yoon TH, Menguy N, Tyliszczak T, Brown GE Jr (2005) Nanoscale environments associated with bioweathering of a

Mg-Fe-pyroxene. *Proceedings of the National Academy of Sciences of the USA* **102**, 979–982.
Benzerara K, Menguy N, Banerjee NR, Tyliszczak T, Guyot F, Brown GE Jr (2007) Alteration of submarine basaltic glass from the Ontong Java Plateau: a STXM and TEM study. *Earth and Planetary Science Letters* **260**, 187–200.
Bernard S, Benzerara K, Beyssac O, Menguy N, Guyot F, Brown GE, Goffé B (2007) Exceptional preservation of fossil plant spores in high-pressure metamorphic rocks. *Earth and Planetary Science Letters* **262**, 257–272.
Bradford MM (1976) A rapid and sensitive method for the quantitation of microgram quantities of protein utilizing the principle of protein-dye binding. *Analytical Biochemistry* **72**, 248–254.
Buffe J, De Vitre RR, Perret D, Leppard GG (1989) Physico-chemical characteristics of a colloidal iron phosphate species formed at the oxic-anoxic interface of a eutrophic lake. *Geochimica et Cosmochimica Acta* **53**, 399–408.
Chaudhuri SK, Lack JG, Coates JD (2001) Biogenic magnetite formation through anaerobic biooxidation of Fe(II). *Applied and Environmental Microbiology* **67**, 2844–2848.
Edwards KJ, Rogers DR, Wirsen CO, McCollom TM (2003) Isolation and characterization of a novel psychrophilic, neutrophilic, chemolithoautotrophic alpha- and gamma-Proteobacteria from the deep sea. *Applied and Environmental Microbiology* **69**, 2906–2913.
Ehrenreich A, Widdel F (1994) Anaerobic oxidation of ferrous iron by purple bacteria, a new type of phototrophic metabolism. *Applied and Environmental Microbiology* **60**, 4517–4526.
Engesgaard P, Kipp KL (1992) A geochemical transport model for redox-controlled movement of mineral fronts in groundwater-flow systems – a case of nitrate removal by oxidation of pyrite. *Water Resources Research* **28**, 2829–2843.
Fejdi P, Poullen J-F, Gasperin M (1980) Affinement de la structure de la vivianite. Fe3(PO4)2·8H_2O. *Bulletin de Mineralogie* **103**, 135–138.
Fortin D, Leppard GG, Tessier A (1993) Characteristics of lacustrine diagenetic iron oxyhydroxides. *Geochimica et Cosmochimica Acta* **57**, 4391–4404.
Frossard E, Bauer JP, Lothe F (1996) Evidence of vivianite in $FeSO_4$-floculated sludges. *Water Research* **31**, 2449–2454.
Hafenbradl D, Keller M, Dirmeier R, Rachel R, Rossnagel P, Burggraf S, Huber H, Stetter KO (1996) Ferroglobus placidus gen nov, sp nov, a novel hyperthermophilic archeum that oxidizes Fe2+ at neutral pH under anoxic conditions. *Archives of Microbiology* **166**, 308–314.
Hansen CBH, Poulsen IF (1999) Interaction of synthetic sulphate ''green rust'' with phosphate and the crystallization of vivianite. *Clays and Clay Minerals* **47**, 312–318.
Heising S, Schink B (1998) Phototrophic oxidation of ferrous iron by a *Rhodomicrobium vannielii* strain. *Microbiology* **144**, 2263–2269.
Hitchcock AP (2001) Soft X-ray spectromicroscopy of polymers and biopolymer interfaces. *Journal of Synchrotron Radiation* **8**, 66–71.
Kappler A, Newman DK (2004) Formation of Fe(III)-minerals by Fe(II)-oxidizing phototrophic bacteria. *Geochimica et Cosmochimica Acta* **68**, 1217–1226.
Kappler A, Schink B, Newman DK (2005) Fe(III) mineral formation and cell encrustation by the nitrate-dependent Fe(II)-oxidizer strain BoFeN1. *Geobiology* **3**, 235–245.
Liu R, Zhao D (2007) *In situ* immobilization of Cu(II) in soils using a new class of iron phosphate nanoparticles. *Chemosphere* **68**, 1867–1876.
Manning PG, Murphy TP, Prepas EE (1991) Intensive formation of vivianite in the bottom sediments of mesotrophic Narrow Lake, Alberta. *Canadian Mineralogist* **29**, 77–85.
Miot J, Benzerara K, Morin G, Kappler A, Bernard S, Obst M, Férard C, Skouri-Panet F, Guigner JM, Posth N, Galvez M, Borwn GE Jr, Guyot F (2009) Iron biomineralization by anaerobic neutrophilic iron-oxidizing bacteria. *Geochimica et Cosmochimica Acta* **73**, 696–711.
Nriagu JO (1972) Stability of vivianite and ion-pair formation in the system $Fe_3(PO_4)_2$-$H_3PO_4H_3PO_4$-H_2O. *Geochimica et Cosmochimica Acta* **36**, 459–472.
Nriagu JO, Dell CI (1974) Diagenetic formation of iron phosphates in recent lake sediments. *American Mineralogist* **59**, 934–946.
Paktunc D, Dutrizac J, Gertsman V (2008) Synthesis and phase transformations involving scorodite, ferric arsenate and arsenical ferrihydrite: implications for arsenic mobility. *Geochimica et Cosmochimica Acta* **72**, 2649–2672.
Postma D, Boesen C, Kristiansen H, Larsen F (1991) Nitrate reduction in an unconfined sandy aquifer-water chemistry, reduction processes, and geochemical modelling. *Water Resources Research* **27**, 2027–2045.
Pratesi G, Cipriani C, Giuli G, Birch WD (2003) Santabarbaraite: a new amorphous phosphate mineral. *European Journal of Mineralogy* **15**, 185–192.
Putnis A, Putnis CV (2007) The mechanism of reequilibration of solids in the presence of a fluid phase. *Journal of Solid State Chemistry* **180**, 1783–1786.
Sapota T, Aldahan A, Al-Aasm I (2006) Sedimentary facies and climate control on formation of vivianite and siderite microconcretions in sediments of Lake Baikal, Siberia. *Journal of Paleolimnology* **36**, 245–257.
Schaedler S, Burkhardt C, Hegler F, Straub KL, Miot J, Benzerara K, Kappler A (2009) Formation of cell-iron-mineral aggregated by phototrophic and nitrate-reducing anaerobic Fe(II)-oxidizing bacteria. *Geomicrobiology Journal* **26**, 93–103.
Schippers A, Jorgensen BB (2002) Biogeochemistry of pyrite and iron sulfide oxidation in marine sediments. *Geochimica et Cosmochimica Acta* **66**, 85–92.
Schwertmann U, Friedl J, Pfab G (1996) A new iron(III) oxyhydroxynitrate. *Journal of Solid State Chemistry* **126**, 336.
Sobolev D, Roden EE (2002) Evidence for rapid microscale bacterial redox cycling of iron in circumneutral environments. *Antonie van Leuwenhoek* **81**, 587–597.
Straub KL, Buchholz-Cleven BEE (1998) Enumeration and detection of anaerobic ferrous iron-oxidizing, nitrate-reducing bacteria from diverse European sediments. *Applied and Environmental Microbiology* **64**, 4846–4856.
Straub KL, Benz M, Schink B, Widdel F (1996) Anaerobic, nitrate-dependent microbial oxidation of ferrous iron. *Applied and Environmental Microbiology* **62**, 1458–1460.
Thole BT, Van der Laan G, Fabrizio M (1994) Magnetic ground state properties and spectral distributions. I. X-ray absorption spectra. *Physical Review. B, Condensed Matter* **50**, 11466–11473.
Ueshima M, Fortin D, Kalin M (2004) Development of iron-phosphate biofilms on pyritic mine waste rock surfaces previously treated with natural phosphate rocks. *Geomicrobiology Journal* **21**, 313–323.
Van der Lee J (1998) Thermodynamical and mathematical concepts of CHESS. Technical Report. LHM/RD/98/39. CIG, Ecole des Mines de Paris, Fontainebleau, France.
Viollier E, Michard G, Jézéquel D, Pèpe M, Sarazin G (1997) Geochemical study of a crater lake: Lake Pavin, Puy de Dôme, France. Constraints afforded by the particulate matter

distribution in the element cycling within the lake. *Chemical Geology* **142**, 225–241.
Viollier E, Inglett PW, Hunter K, Roychoudhury AN, Van Cappellen P (2000) The ferrozine method revisited: Fe(II)/Fe(III) determination in natural waters. *Applied Geochemistry* **15**, 785–790.
Von Guten U, Schneider W (1991) Primary products of oxygenation of iron(II) at an oxic-anoxic boundary: nucleation, aggregation and aging. *Journal of Colloid and Interface Science* **145**, 127–139.
Webb S (2004) SIXPACK: a graphical user interface for XAS analysis using IFEFFIT. *Physica Scripta* **115**, 1011–1014.
Weber KA, Picardal FW, Roden EE (2001) Microbially catalyzed nitrate-dependent oxidation of biogenic solid-phase Fe(II) compounds. *Environmental Science and Technology* **35**, 1644–1650.
Widdel F, Schnell S, Heising S, Ehrenreich A, Assmus B, Schink B (1993) Ferrous iron oxidation by anoxygenic phototrophic bacteria. *Nature* **362**, 834–836.
Wilke M, Farges F, Petit PE, Brown GE Jr, Martin F (2001) Oxidation state and coordination of Fe in minerals: An Fe *K*-XANES spectroscopic study. *American Mineralogist* **86**, 714–730.
Winterer M (1997) XAFS – A data analysis program for material science. *Journal of Physics IV* **7**, 243–244.

SUPPORTING INFORMATION

Additional supporting information may be found in the online version of this article:

Figure S1 Beam radiation damage on reference Fe(II)-phosphate (A) and on Fe(III)-encrusted bacteria (B). Evolution of the Fe(III)/Fe(total) ratio as function of dwell time, estimated by fitting Fe $L_{2,3}$-edges NEXAFS spectra recorded on reference Fe(II)-phosphate and Fe(III)-encrusted bacteria, respectively.

Figure S2 STEM images of BoFeN1 cells grown in the presence of vivianite (V). (A) BoFeN1 cell with encrusted periplasm (p). (B) BoFeN1 cells with membrane-bound globules (g).

Data S1 Details on XAS data acquisition and on the EXAFS data fitting procedure.

Please note: Wiley-Blackwell are not responsible for the content or functionality of any supporting materials supplied by the authors. Any queries (other than missing material) should be directed to the corresponding author for the article.